Available online at www.sciencedirect.com
ScienceDirect
Ceramics International 38 (2012) 217–222
CERAMICS INTERNATIONAL
www.elsevier.com/locate/ceramint

Electric current assisted sintering of continuous functionally graded Ti_2AlN/TiN material

Yi Liu *, Zhihao Jin

State Key Laboratory for Mechanical Behavior of Materials, Xi'an Jiaotong University, 710049 Xi'an, PR China

Received 18 May 2011; received in revised form 27 June 2011; accepted 28 June 2011
Available online 2nd July 2011

Abstract

A Ti/AlN powder mixture with a molar ratio of 2:1 was consolidated by electric current assisted sintering (ECAS) using a special designed graphite die which can give rise to a huge temperature gradient along the vertical direction in the sintering compact. By this way, a continuous microstructural evolution during the formation of Ti_2AlN was observed. At 1200 °C, a Ti_2AlN–TiN composite was prepared through the in situ decomposition of Ti_2AlN. The SEM and XRD results revealed that a continuous variation of Ti_2AlN and TiN phase content was achieved. The gradual hardness distribution across the entire composite further indicated that a continuous functionally graded Ti_2AlN/TiN material was obtained rapidly by taking advantage of the ECAS method.

Keywords: B. Composites; C. Hardness; D. Nitride; E. Structural application

1. Introduction

In order to reduce the stress concentration in a component when it suffers rigorous conditions such as rapid heating or cooling and sudden impact, a transitional layer between different materials is usually introduced. This gives the birth of the functionally graded materials (FGMs) [1]. The FGMs are usually composites in which the composition and/or microstructure vary gradually along one, two or three dimensions [2]. There are numerous methods to process FGMs, such as casting [3], laser cladding [4], combustion synthesis [5] and powder metallurgy [6]. Among these, the powder metallurgy technique is one of the most important ways since it can be easily accomplished by stacking material ingredients into layers through a variety of methods [1,2]. However, the partial sintering of different layers may compromise the reliability of the component under operating conditions since layers with different compositions need different temperatures to be fully densified. Therefore, to overcome this problem, new approaches must be considered.

Over the last decades, electric current assisted sintering (ECAS), also known as spark plasma sintering (SPS), has been extensively used for synthesis or consolidation of various materials. The rapid heating rate and possible plasma during ECAS make it possible to fabricate materials at low temperature and with short periods of time. Although a temperature gradient always exists inside the die and specimen due to the intrinsic heating method [7,8], it can be minimized by the careful process, such as using the highly symmetrical heating set-up together with adiabatic materials around the die and taking the multi-stepped heating rate [9,10]. In the most cases, the temperature gradient is minimized in order to prepare homogeneous materials. However, from a different point of view, the temperature gradient can be enlarged if the heating set-up departs from the high symmetry. Based on this idea, several attempts have been done to fabricate the FGMs by designing the heating set-up [11–15]. For example, Hong et al. [12] prepared ZrB_2–SiC/ZrO_2(3Y) FGM by using an unsymmetrical graphite die. In that work, every layer with the different contents of the ZrB_2 and SiC/ZrO_2(3Y) was fully densified because of the temperature gradient. Compared with Hong's work, Hulbert et al. [13,14] fabricated the B_4C/Al FGM with a continuous gradation of microstructure and thus performed increased mechanical properties. Lately, Belmonte et al. [15] used temperature gradient to control the phase transformation of Si_3N_4. They achieved a continuous gradient of α/β phase contents and grain sizes from a sole homogeneous

* Corresponding author. Tel.: +86 29 82665221; fax: +86 29 82665443.
E-mail address: liuyi.0825@gmail.com (Y. Liu).

0272-8842/$36.00
doi:10.1016/j.ceramint.2011.06.053

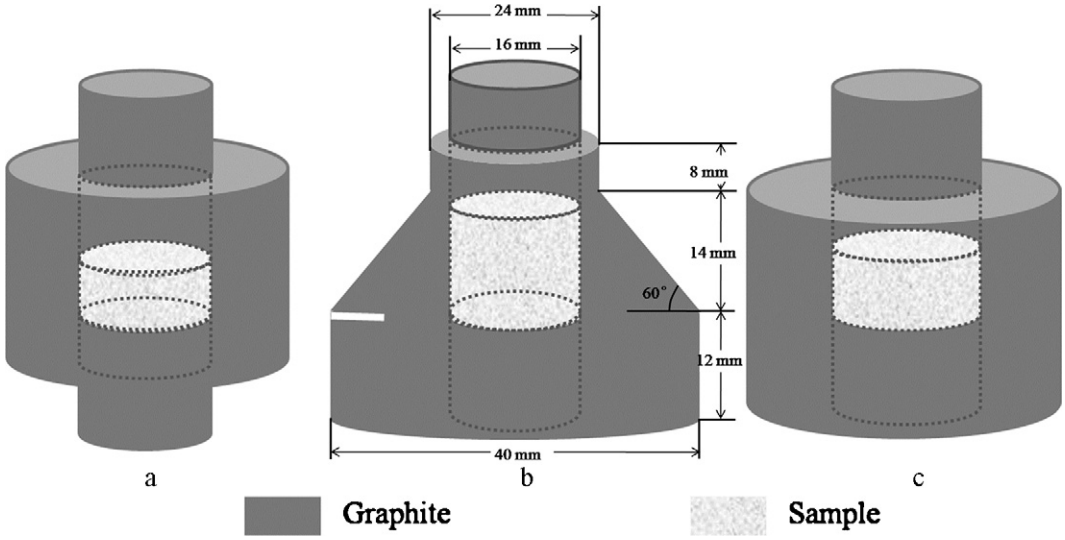

Fig. 1. Graphite moulds with three different shapes used in ECAS. (a) For homogeneous temperature distribution; (b) and (c) for gradient temperature distribution.

starting powder. The possibility of designing a temperature gradient into the material during sintering opens a new window for synthesizing FGMs by ECAS.

The Ti_2AlN/TiN FGM is considered as a promising composite to be used in high-strength armour and high-abrasive conditions due to the high strength and stiffness of the TiN phase combined with the tough and ductile Ti_2AlN [16,17]. However, to our best knowledge, few studies on the preparation of Ti_2AlN/TiN FGM by any method have been reported. In the present work, the Ti/AlN powder mixture was adopted to synthesize the Ti_2AlN/TiN FGM by ECAS using a special designed graphite mould and the continuous microstructural evolution during the reaction sintering of Ti and AlN was studied.

2. Experimental

Commercial Ti (particle size: 25 μm; purity: 99.5%) and AlN (particle size: 3 μm; purity: 99.2%) powders were used as raw materials. The powder mixtures, having a stoichiometric Ti to AlN molar ratio of 2:1, were ball-milled for 12 h in an air-sealed container with a ball to powder mass ratio of 4:1. The powder mixture was then dried, sieved (100 mesh) and filled into the designed graphite mould which is shown in Fig. 1(b). The subsequent sintering was carried out in the vacuum of 6 Pa by the ECAS apparatus (ED-PASIII, Elenix). A heating rate of 100 °C/min and a uniaxial pressure of 30 MPa were applied. The temperature was regulated and controlled by an infrared pyrometer that was focused on the hole labelled on the graphite die. In order to investigate the reaction between Ti and AlN, the powder compacts were heated to 900 °C, 1000 °C, 1100 °C and cooled down immediately with the cooling rate >200 °C. Finally, the Ti_2AlN/TiN FGM was prepared at 1200 °C with holding time of 3 min. The sintered samples had diameters of 16 mm and heights of 10 mm. In order to eliminate the graphite contamination, the surfaces of the samples were ground down 1 mm.

Before characterization, the samples were cut into small pieces with different shapes by electric discharge machining (EDM). The surfaces of the pieces were polished down to 1 μm, finishing by diamond paste. The X-ray diffraction (XRD) was conducted on the polished surface with a PANnalytical X'Pert, using Cu $K_{\alpha 1}$ radiation at 45 kV and 40 mA. The microstructures were observed by Scanning Electron Microscopy (SEM, S-2700) and Optical Microscopy (OM, MEF-3). For the OM, the polished pieces were etched with an acidic solution (HNO_3:HF:H_2O = 1:1:2). The hardness across the sample was tested by Vickers indentation method using an external force of 9.8 N and holding for 15 s. Five indents were taken at the equivalent position.

Fig. 2. Real-time colour distribution of graphite mould during the sintering. Note that the white, yellow and red colour represent high, intermediate and low temperature respectively. (For interpretation of the references to colour in this figure legend, the reader is referred to the web version of the article.)

3. Results and discussion

3.1. The design of the graphite die and observation of temperature gradient

The heating in the ECAS is based on the Joule effect. The current passes through the mould (usually made of graphite) or the material (if it is conductive). So the temperature distribution inside the die and the sample is dependent on the resistance of different parts of the whole set-up. Graphite dies with three different shapes are usually adopted in ECAS under the normal pressure as shown in Fig. 1. The die with highest symmetry along the vertical and horizontal directions is given in Fig. 1(a). It gives a relative homogeneous temperature distribution inside the sample because heating from the upper punch and lower punch is equivalent. However, when the symmetry along the vertical direction is broken, as shown in Fig. 1(b) and (c), a temperature gradient is supposed to be present due to the unsymmetrical heating from the upper parts. The graphite die with the shape as shown in Fig. 1(b) is adopted in this work since the die with the gradual change along the lateral direction may give rise to a larger and smoother temperature gradient. The real-time photograph during ECAS is shown in Fig. 2. The colour changes along the vertical direction are an indication of different temperatures. It is noticeable that Fig. 2 shows smoother temperature gradient than Ref. [14] in which the graphite die with the shape as shown in Fig. 1(c) was adopted. It is also clear from Fig. 2 that it is difficult to measure the temperature within the graphite die. It is even harder to consider the real temperature inside the specimen and further numerical modelling is needed.

3.2. Continuous evolution of microstructure during the reaction sintering of Ti and AlN

The microstructures of the samples heated to 900 °C, 1000 °C, and 1100 °C without holding time are presented in Fig. 3. The rapid cooling rate (>200 °C/min) enables the

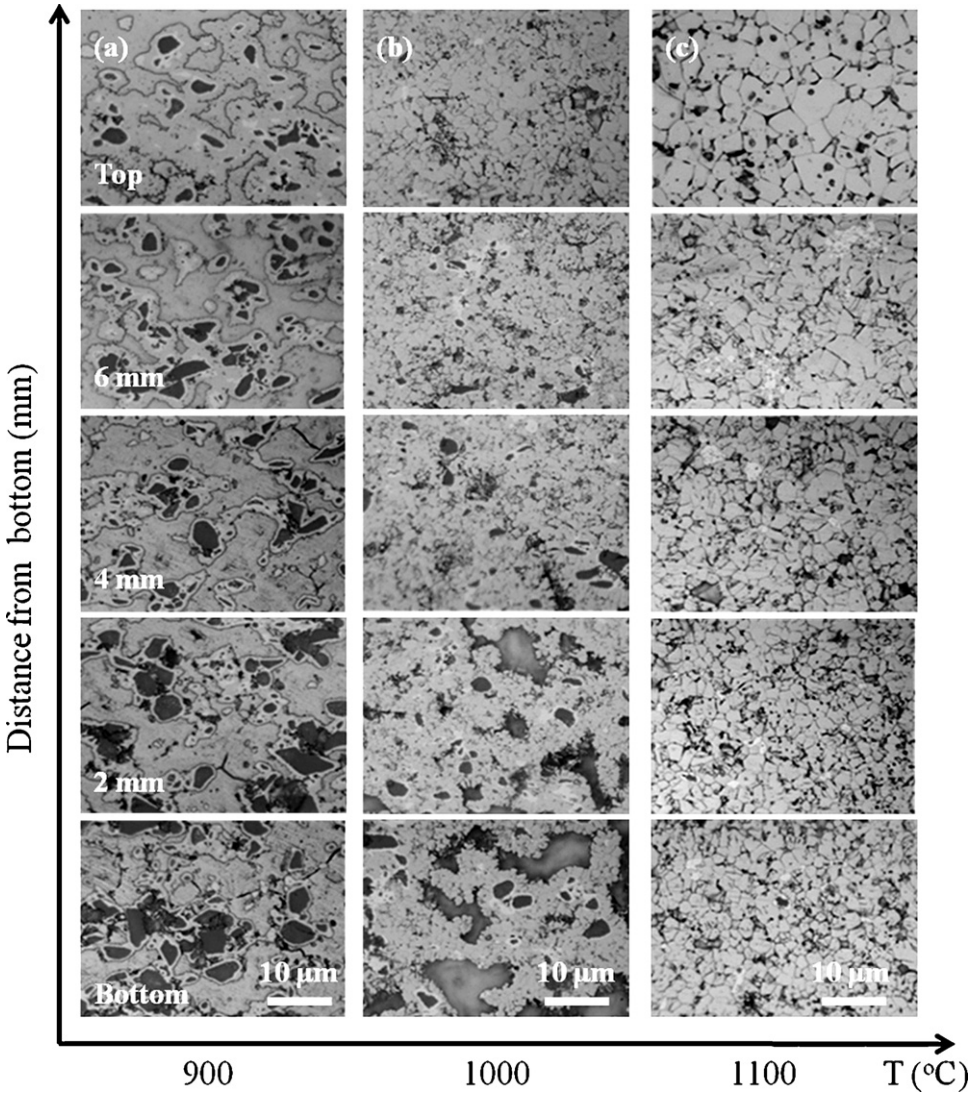

Fig. 3. Optical micrographs of polished and chemically etched specimens sintered at (a) 900 °C, (b) 1000 °C and (c) 1100 °C. The images were taken at increasing distances (2 mm steps) from the bottom surface.

''freeze'' of the real-time microstructure and therefore, it is possible to follow the real-time evolution of microstructure during the reaction sintering of Ti and AlN. The darkest contrast in Fig. 3(a) was identified by EDS to be AlN. It can be seen that more AlN particles are present in the bottom of the sample where the temperature is lower. As the distance from the bottom increases, the size of the AlN particles becomes smaller and thus its content decreases. Simultaneously, a reaction zone, having the ''islands'' shape, forms and grows around AlN grains gradually. So in this stage, it can be concluded that the main reaction is the diffusion of AlN. When the temperature increased to 1000 °C (Fig. 3(b)), there are still some AlN particles embedded in the newly formed phases until in the top surface of the sample, where few AlN particles can be found and some new phases with the equiaxed shape are present. Therefore, the main feature of this stage is also the diffusion of AlN. From the microstructures of the sample heated to 1100 °C (Fig. 3(c)), it is obvious that the grain size grows up gradually from the bottom to the top of the sample. So in this stage, the reaction (if not finished yet) should be accompanied by the grain growth.

In order to understand the microstructural evolution deeply, the phase analysis of the bottom and top surfaces of the samples heated to 900 °C, 1000 °C and 1100 °C were conducted by XRD. The results are shown in Fig. 4. Several intermediate phases, such as TiN, Ti_3Al, Ti_3AlN and TiAl, are presented in the spectrums which reveals a reaction pathway towards the formation of Ti_2AlN. A detailed analysis of reaction process is beyond the scope of this paper and has been reported elsewhere [18]. However, it should be mentioned that the sintering with designed temperature gradient offers an efficient way to study the reaction between Ti and AlN. It is possible to obtain reaction information from several hundreds of degrees by only three samples on the contrary to conventional methods where lots of samples with different sintering temperatures are required. Furthermore, the information derived from the samples prepared by the conventional methods is discrete and as a result, the important reaction details may be overlooked, especially when the reaction is complicated. Therefore, the method applied in this work is not only favourable for the Ti/AlN system but also applicable for other reaction systems.

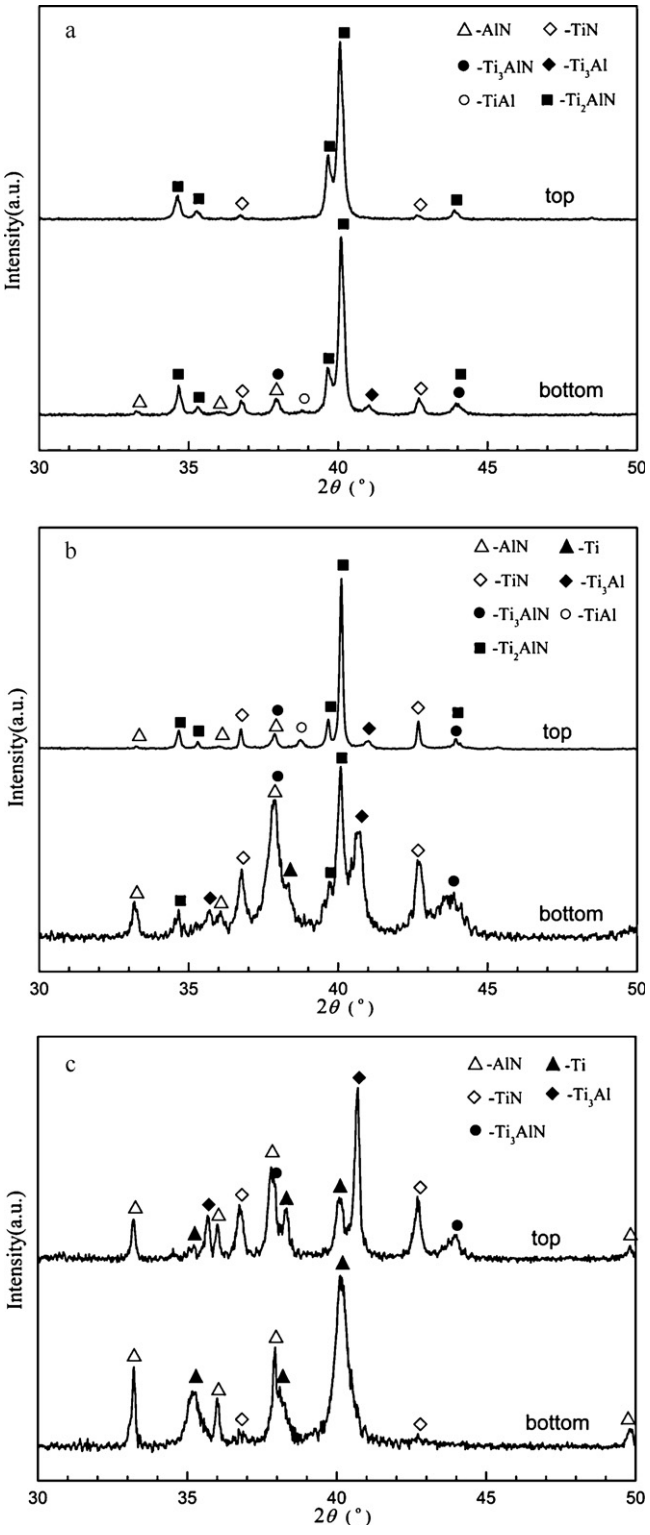

Fig. 4. XRD patterns from the top and bottom surfaces of specimens sintered at (a) 1100 °C, (b) 1000 °C and (c) 900 °C.

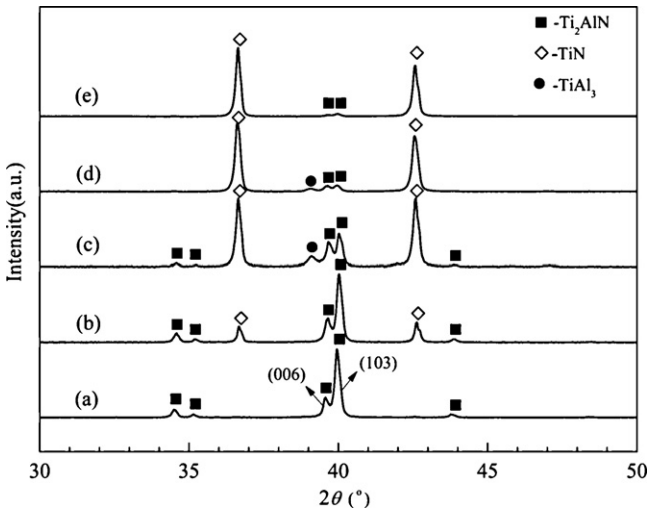

Fig. 5. XRD patterns from different layers of the specimen sintered at 1200 °C for 3 min. (a) Bottom surface, (b) 2 mm from bottom, (c) 4 mm from bottom, (d) 6 mm from bottom and (e) top surface.

3.3. Functionally graded Ti_2AlN/TiN material

The sample sintered at 1100 °C showed mainly Ti_2AlN phase at the top surface as shown in Fig. 4(a). So it is expected that the phase decomposition of Ti_2AlN occurs when the sample is heated over 1100 °C. The XRD patterns from different layers of the specimen sintered at 1200 °C are shown in Fig. 5. It is seen that the relative intensity of the Ti_2AlN phase decreases as the distance from the bottom of the sample increases. The opposite is seen for the TiN phase. It is noted that the $TiAl_3$ phase appears in the middle of the specimen and its relative intensity decreases gradually towards to the top surface. It should be also noted that the relative intensities of (0 0 6) and (1 0 3) planes of Ti_2AlN changes at different layers.

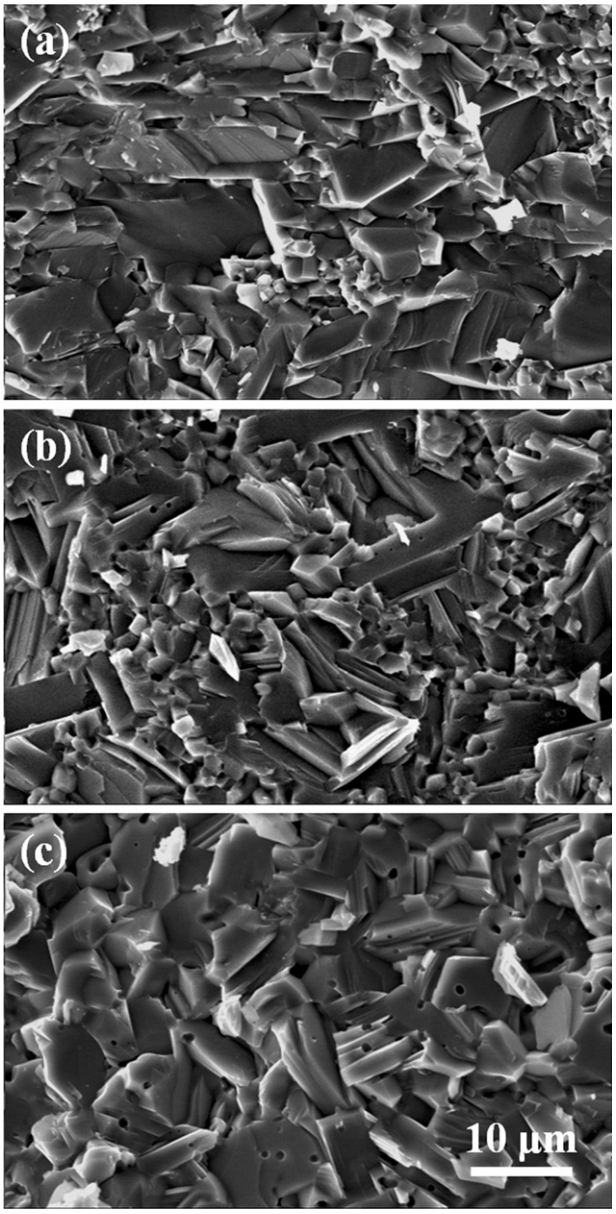

Fig. 6. SEM micrographs of the specimen sintered at 1200 °C for 3 min. The images were taken from different positions of the fractural surface: (a) near top surface, (b) in the middle and (c) near bottom surface.

The microstructures of different layers are shown in Fig. 6. It can be seen that at the bottom layer the sample (Fig. 6(c)) is composed of the grains with equiaxed shape. Combined with the XRD patterns in Fig. 5(a), it can be interpret that these grains are single-phase Ti_2AlN. However, it should be noted that the small pores are present inside the Ti_2AlN grains. This may attribute to the unfinished dehydrogenation of Ti powder and thus, the hydrogen was released and entrapped in the grains during the sintering. In the middle part of the specimen, the microstructure shows a bimodal distribution: the large elongated grains and small equiaxed grains. However, when come to the top surface, as Fig. 6(c) shows, the grains with square shape constitute the main part of the sample. Based on the XRD and SEM analysis, it is obvious that the decomposition of Ti_2AlN has occurred and a functionally graded Ti_2AlN/AlN material is obtained by sintering at 1200 °C.

The lattice structure of the Ti_2AlN can be simply regarded as the alternate stacking of Ti–Al layer and Ti–N layer [19]. A possible process for the decomposition of Ti_2AlN can be proposed as follows: Ti–Al layer is firstly broken when the Ti_2AlN suffers high temperature and the Al atoms dissolve in the Ti_2AlN lattice as its content is small. At this period, the lattice of Ti_2AlN sustains its own structure. That is why only TiN and Ti_2AlN phases are identified in Fig. 5(b). When the decomposition becomes severer, more Al atoms are released and $TiAl_3$ forms. As a result, part of the Ti_2AlN lattice collapse and thus the relative intensities of different peaks of Ti_2AlN are changed which can be reflected from Fig. 5(c). Furthermore, as the Ti_2AlN lattice collapses, the morphology of Ti_2AlN grains is also changed, as seen in Fig. 6(b). Once the $TiAl_3$ forms, it can be easily squeezed out from the graphite die under the uniaxial pressure and therefore, its content decreases from the middle towards to the top of the specimen as shown from Fig. 5(c) to (e). Finally, at the top, only TiN with a minor amount of Ti_2AlN can be found (Fig. 5(e)).

It is known that the Ti_2AlN has a low hardness, about 3.9 GPa according to this work and the TiN has a high hardness, about 21 GPa from Ref. [20]. Therefore, the hardness of their composite should lie between 3.9 GPa and 21 GPa. The

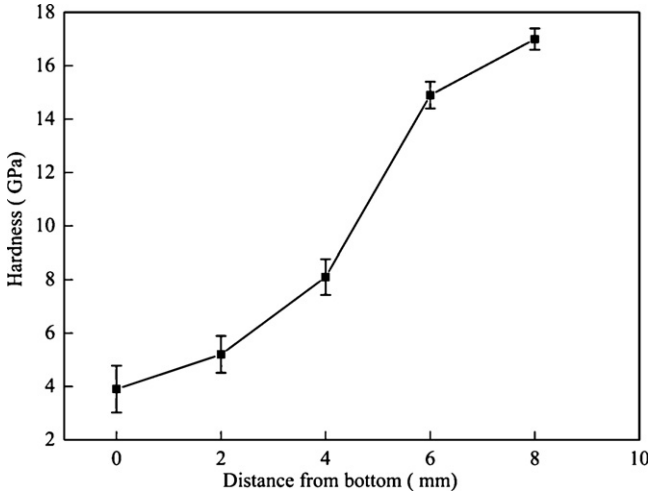

Fig. 7. Hardness distribution across the sample sintered at 1200 °C for 3 min.

measured hardness values across the specimen are shown in Fig. 7. As expected, the hardness shows a minimum value (3.9 GPa) at the bottom surface of the specimen where the main phase is single Ti_2AlN. And the maximum value (17 GPa) is present at the top surface of the specimen where the main phase is TiN. Moreover, the hardness values show a gradual variation from the bottom to the top surface. This kind of continuous distribution makes the Ti_2AlN/TiN FGM applicable for the structural aspect where the TiN side can resist impact or abrasion and the Ti_2AlN can release the internal stresses and thus increases the reliability of the whole composite.

4. Conclusions

A large temperature gradient was obtained by designing the graphite mould used in the ECAS process. By this technique, the functional graded materials in the Ti–Al–N system have been fabricated. This also offered an effective way to study the reaction between Ti and AlN by observing the continuous evolution of the microstructure. Furthermore, the Ti_2AlN/TiN FGM with a continuous hardness distribution has been prepared by the in situ decomposition of Ti_2AlN. This approach provides an easy method to design the FGMs and further extends the applications of the ECAS technique.

Acknowledgements

The authors thank Dr. Shi and Dr. Eriksson for the revision of manuscript.

References

[1] S. Suresh, A. Mortensen, Fundamentals of Functionally Graded Materials, IOM Communications Ltd., London, 1998.
[2] B. Kieback, A. Neubrand, H. Riedel, Processing techniques for functionally graded materials, Mater. Sci. Eng. A 362 (2003) 81–106.
[3] J.G. Yeo, Y.G. Jung, S.C. Choi, Design and microstructure of ZrO_2/SUS316 functionally graded materials by tape casting, Mater. Lett. 37 (1998) 304–311.
[4] Y.T. Pei, T.C. Zuo, Gradient microstructure in laser clad TiC-reinforced Ni-alloy composite coating, Mater. Sci. Eng. A 241 (1998) 259–263.
[5] M. Cirakoglu, S. Bhaduri, S.B. Bhaduri, Combustion synthesis processing of functionally graded materials in the Ti–B binary system, J. Alloy Compd. 347 (2002) 259–265.
[6] H.X. Zhu, R. Abbaschian, Microstructures and properties of in-situ NiAl–Al_2O_3 functionally gradient composites, Compos. Part B 31 (2000) 383–390.
[7] U. Anselmi-Tamburini, S. Gennari, J.E. Garay, Z.A. Munir, Fundamental investigations on the spark plasma sintering/synthesis process. II. Modeling of current and temperature distributions, Mater. Sci. Eng. A 394 (2005) 139–148.
[8] K. Vanmeensel, A. Laptev, J. Hennicke, J. Vleugels, O. Van der Biest, Modelling of the temperature distribution during field assisted sintering, Acta Mater. 53 (2005) 4379–4388.
[9] M. Suganuma, Y. Kitagawa, S. Wada, N. Murayama, Pulsed electric current sintering of silicon nitride, J. Am. Ceram. Soc. 86 (2003) 387–394.
[10] K. Madhav Reddy, N. Kumar, B. Basu, Innovative multi-stage spark plasma sintering to obtain strong and tough ultrafine-grained ceramics, Scr. Mater. 62 (2010) 435–438.
[11] M.J. Suk, S.I. Choi, J.S. Kim, Y.D. Kim, Y.S. Kwon, Fabrication of a porous material with a porosity gradient by a pulsed electric current sintering process, Met. Mater. Int. 9 (2003) 599–603.
[12] C.Q. Hong, X.H. Zhang, W.J. Li, J.C. Han, S.H. Meng, A novel functionally graded material in the ZrB_2–SiC and ZrO_2 system by spark plasma sintering, Mater. Sci. Eng. A 498 (2008) 437–441.
[13] D.M. Hulbert, D.T. Jiang, U. Anselmi-Tamburini, C. Unuvar, A.K. Mukherjee, Continuous functionally graded boron carbide-aluminum nanocomposites by spark plasma sintering, Mater. Sci. Eng. A 493 (2008) 251–255.
[14] D.M. Hulbert, D.T. Jiang, U. Anselmi-Tamburini, C. Unuvar, A.K. Mukherjee, Experiments and modeling of spark plasma sintered, functionally graded boron carbide–aluminum composites, Mater. Sci. Eng. A 488 (2008) 333–338.
[15] M. Belmonte, J. Gonzalez-Julian, P. Miranzo, M.I. Osendi, Continuous in situ functionally graded silicon nitride materials, Acta Mater. 57 (2009) 2607–2612.
[16] M.W. Barsoum, M. Ali, T. El-Raghy, Processing and characterization of Ti_2AlC, Ti_2AlN, and $Ti_2AlC_{0.5}N_{0.5}$, Metall. Mater. Trans. A 31 (2000) 1857–1865.
[17] Z.J. Lin, M.J. Zhuo, M.S. Li, J.Y. Wang, Y.C. Zhou, Synthesis and microstructure of layered-ternary Ti_2AlN ceramic, Scr. Mater. 56 (2007) 1115–1118.
[18] Y. Liu, Z.Q. Shi, J.P. Wang, G.J. Qiao, Z.H. Jin, Z.J. Shen, Reactive consolidation of layered-ternary Ti_2AlN ceramics by spark plasma sintering of a Ti/AlN powder mixture, J. Eur. Ceram. Soc. 31 (2011) 863–868.
[19] M.W. Barsoum, The M_{N+1} AX_N phases: a new class of solids; thermodynamically stable nanolaminates, Prog. Solid State Chem. 28 (2000) 201–281.
[20] H. Ljungcrantz, M. Odén, L. Hultman, J.E. Greene, J.E. Sundgren, Nanoindentation studies of single-crystal (0 0 1)-, (0 1 1)-, and (1 1 1)-oriented TiN layers on MgO, J. Appl. Phys. 80 (1996) 6725–6733.